An Avidity-based PD-L1 Antagonist Using Nanoparticle-Antibody Conjugates for Enhanced Immunotherapy

*Jiyoon Bu[1], Ashita Nair[1], Mari Iida[2], Woo-jin Jeong[1], Michael J. Poellmann[1], Kara Mudd[1], Luke J. Kubiatowicz[1], Elizabeth W. Liu[1], Deric L. Wheeler[2,3], and Seungpyo Hong[1,3,4]**

1 Pharmaceutical Sciences Division, School of Pharmacy, University of Wisconsin-Madison, Madison, WI 53705, USA

2 Department of Human Oncology, School of Medicine and Public Health, University of Wisconsin-Madison, Madison, WI 53705, USA

3 Carbone Cancer Center, School of Medicine and Public Health, University of Wisconsin-Madison, Madison, WI 53705, USA

4 Yonsei Frontier Lab and Department of Pharmacy, Yonsei University, Seoul 03722, Republic of Korea

*Address all correspondence to:

Prof. Seungpyo Hong
Pharmaceutical Sciences Division, School of Pharmacy, University of Wisconsin – Madison
7121 Rennebohm Hall 777 Highland Avenue, Madison, WI 53705, USA
email: seungpyo.hong@wisc.edu / phone: (608) 890-0699

KEYWORDS

immunotherapy, multivalent binding, PD-1/PD-L1 interaction, dendrimer, immune checkpoint inhibitor

ABSTRACT

Upregulation of programmed death ligand 1 (PD-L1) allows cancer cells to evade antitumor immunity. Despite tremendous efforts in developing PD-1/PD-L1 immune checkpoint inhibitors (ICIs), clinical trials using such ICIs have shown inconsistent benefits. Here, we hypothesized that the ICI efficacy would be dictated by the binding strength of the inhibitor to the target proteins. To assess this, hyperbranched, multivalent poly(amidoamine) dendrimers were employed to prepare dendrimer-ICI conjugates (G7-aPD-L1). Binding kinetics measurements using SPR, BLI, and AFM revealed that G7-aPD-L1 exhibits significantly enhanced binding strength to PD-L1 proteins, compared to free aPD-L1. The binding avidity of G7-aPD-L1 was translated into *in vitro* efficiency and *in vivo* selectivity, as the conjugates improved the PD-L1 blockade effect and enhanced accumulation in tumor sites. Our results demonstrate that the dendrimer-mediated multivalent interaction substantially increases the binding avidity of the ICIs and thereby improves the antagonist effect, providing a novel platform for cancer immunotherapy.

TABLE OF CONTENTS FIGURE

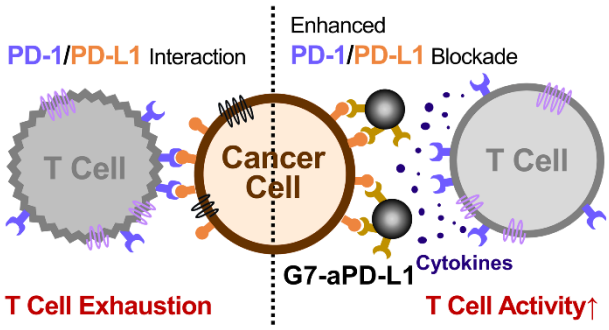

MAIN TEXT

The immune system is responsible for the detection of abnormal cells and suppression of their rapid growth.[1] Activation of the innate immune system stimulates T cells to attack malignant tumor cells.[2] However, tumor cells frequently adapt to evade immune surveillance and interfere with the T cell response by triggering immune checkpoint regulators. This causes a dysregulation of the antitumor immune response, thereby exhibiting immune-inhibitory behaviors.[3-5] Cancer immunotherapy is a burgeoning treatment that restores and/or reactivates the immune system via blockade of the immune checkpoint pathways.[6] A number of immune checkpoint inhibitors (ICIs) have been developed to modulate these pathways through the targeting of immunosuppressive molecules, notably the interaction between programmed death ligand 1 (PD-L1) on cancer cells and its counter receptor PD-1 on T cells.[7-11]

PD-L1 is a bidirectional membrane protein that is widely expressed in many cancer types, including ovarian cancer, renal cell carcinoma, hepatocellular carcinoma, and lung cancer.[12-16] Its interaction with PD-1 receptors disrupts the natural immune response mounted against

tumors. This has led to the development of several PD-L1 specific antagonists, primarily in a form of monoclonal antibodies, which include three FDA-approved drugs, Atezolizumab, Avelumab, and Durvalumab.[17] However, the currently available PD-L1-targeted immunotherapy agents have faced considerable challenges in clinical trials, due to heterogeneity of PD-L1 expressions in tumor, active redistribution of the ligand after the treatment, and low target efficacy or binding strength of the prevalent antibody drugs.[18-23]

In this study, we hypothesized that the integration of dendrimer nanoparticles with ICI antibodies would enhance the binding avidity of the PD-L1 antagonists, substantially increasing the therapeutic efficacy (**Scheme 1**). Note that we previously reported that dendrimers effectively facilitate multivalent binding, as evidenced by significant reduction in dissociation rate and enhancement in surface targeting.[24-27] This was attributed to the unique capability of dendrimers that accommodate multiple ligands on its nanoscale surface area and that deforms to enable the conformational optimization of the multiple ligands to bind to their counterparts simultaneously.[24, 28] Based on these, we assess the following specific hypotheses in this study: i) conjugation of ICIs to dendrimers would result in a significant increase in binding kinetics; ii) the increased binding kinetics would in turn improve *in vitro* efficiency and *in vivo* tumor accumulation of the ICI-dendrimer conjugates.

To test these hypotheses, we designed a nanoparticle drug delivery platform consisting of generation 7 (G7) poly(amidoamine) (PAMAM) dendrimers conjugated with multiple PD-L1-targeting molecules per dendrimer (G7-aPD-L1). The G7-aPD-L1 conjugates were synthesized as described in **Figure 1A**. G7 PAMAM dendrimers were first labeled with Alexa Fluor 647 (AF_{647}). The dendrimers were then reacted with acetic anhydride to obtain primary amine acetylation. Approximately 75-90% of the peripheral functional groups were acetylated to

provide a more neutral surface charge.[29] The remaining amine groups on the partially acetylated dendrimers were subsequently carboxylated through the reaction with succinic anhydride. The presence of the different terminal groups after each chemical reaction was confirmed using proton nuclear magnetic resonance (^{1}H NMR), as shown in **Figure S1**. Following the surface modification, the dendrimers were activated with N-hydroxysuccinimide (NHS) and subsequently reacted with anti-PD-L1 human antibodies (aPD-L1$_h$) at a molar ratio of 1:5. Samples were then purified using centrifugal filters in order to remove unconjugated reactants.

The final G7-aPD-L1$_h$ conjugates were comprised of 3.7 ± 0.5 antibodies per dendrimer, as assessed using a bicinchoninic acid (BCA) assay and fluorescent intensity measurements (**Figure S2**). The molar ratio of impurities, including free aPD-L1$_h$ or unconjugated dendrimers, to the anticipated conjugates (G7-aPD-L1$_h$) was confirmed to be less than 3% (**Figure 1B and S2**). The G7-aPD-L1$_h$ conjugates were further characterized using atomic force microscopy (AFM) and gel permeation chromatography (GPC). The AFM images revealed that the diameter (D) and height (h) of the G7-aPD-L1$_h$ conjugates were significantly larger (D = 27.4 ± 8.9 nm and h = 9.8 ± 3.9 Å) than those of free antibodies (D = 12.7 ± 4.4 nm; $p < 0.001$ and h = 6.7 ± 2.5 Å; $p < 0.001$) and unconjugated dendrimers (D = 16.3 ± 7.3 nm; $p < 0.001$ and h = 5.6 ± 1.6 Å; $p < 0.001$) (**Figure 1C-E**). Note that the differences in height and diameter imply the flattening of the nanoparticles on the mica surface, which was also reported elsewhere.[30] The GPC chromatograms of the G7-aPD-L1$_h$ conjugates, unmodified dendrimers, and aPD-L1$_h$ (**Figure S3**) further supported successful conjugation between antibodies and dendrimers. At the detection wavelength of 280 nm (characteristic to proteins), the G7-aPD-L1$_h$ conjugates displayed a faster elution time compared to aPD-L1$_h$ (21.9 ± 0.4 min vs. 23.0 ± 0.1 min; p = 0.007), confirming the increased molecular weight of the conjugates. Furthermore, area under

the peak from the conjugates was larger than that from the free antibody by ~3.6-fold, indicating that ~3.6 antibodies were conjugated to each of the dendrimers, which is consistent with the results obtained using the BCA assay.

The binding kinetics of the dendrimer-ICI conjugates to PD-L1 was quantitatively analyzed using three direct measurement methods: biolayer interferometry (BLI), surface plasmon resonance spectroscopy (SPR), and AFM. Binding affinities determined using PD-L1-functionalized BLI probes demonstrated that the G7-aPD-L1$_h$ conjugates interact more strongly with PD-L1 molecules than aPD-L1$_h$ (**Figure 2A**). The G7-aPD-L1$_h$ conjugates showed an average dissociation constant (K_D) of $(8.5 \pm 2.3) \times 10^{-11}$ M, which was an order of magnitude lower than the K_D obtained from aPD-L1$_h$ ($(9.6 \pm 1.7) \times 10^{-10}$ M; $p = 0.016$), at inhibitor concentrations between 6.25 and 25.0 μg/mL. Binding affinity was further assessed using SPR, by infusing the inhibitors through the protein-immobilized SPR chip at a flow rate of 10 μL/min (**Figure 2B**). The G7-aPD-L1$_h$ conjugates exhibited 5.8-fold enhanced binding avidity with PD-L1, compared to free aPD-L1$_h$ ($(6.6 \pm 2.7) \times 10^{-11}$ M vs. $(3.8 \pm 1.0) \times 10^{-10}$ M; $p = 0.007$).

The lower K_D of the G7-aPD-L1$_h$ conjugates, compared to those of free aPD-L1$_h$ were most likely attributed to their faster association (k_{on}) with the target proteins (**Table S1** and **S2**). In contrast, the difference in off-rate kinetics between the two inhibitors was not prominent. Both the G7-aPD-L1$_h$ conjugates and aPD-L1$_h$ demonstrated significantly slow dissociation (k_{off}) at inhibitor concentrations of 6.25 - 25.0 μg/mL, ($(1.4 \pm 0.6) \times 10^{-4}$ s^{-1} vs. $(2.6 \pm 0.2) \times 10^{-4}$ s^{-1}; BLI). The more sensitive AFM force spectroscopy was thus employed to resolve the difference in dissociation kinetics of the two inhibitors, as the multivalent binding typically results in a significant reduction in k_{off} (**Figure 2C**).[24, 31-35] The detailed description for the preparation steps are provided in **Supporting Information**. Representative force-distance (FD) curves obtained

from aPD-L1$_h$- and G7-aPD-L1$_h$-functionalized surfaces at a loading rate of 1,160 nN/s are shown in **Figure 2D**. Multivalent interaction between the G7-aPD-L1$_h$ conjugates and PD-L1 was identified from the FD curves, as represented by two or more discrete unbinding events (rupture force >50 pN) occurring at a retraction phase. These multivalent interactions were more frequently found from the G7-aPD-L1$_h$ conjugates than aPD-L1$_h$ (**Table S3**), and for the both inhibitors, the maximum adhesion forces and energies obtained from the curves with multiple unbinding events were significantly larger than those obtained from single unbinding events, regardless of the loading rate (**Table S4-S7**).

As a result, the average of mean maximum adhesion forces on four G7-aPD-L1$_h$-functionalized surfaces ranged from 301 - 376 pN, depending on the pulling velocity (1 - 20 μm/s) (**Figure 2E** and **S4**). These were 1.2- to 1.3-fold stronger than the forces obtained from the aPD-L1$_h$ surfaces (225 - 320 pN) at the same pulling velocity. The differences in dissociation kinetics were more pronounced when comparing the adhesion energies (**Figure 2F**). The energies ranged from 11.7-27.0 pN·μm and 3.9-13.0 pN·μm for the G7-aPD-L1$_h$ conjugates and aPD-L1$_h$, respectively. The force spectrum of the G7-aPD-L1$_h$ conjugates versus aPD-L1$_h$ was further analyzed using the Bell-Evans model (**Figure 2G**).[36] The k_{off} of the G7-aPD-L1$_h$ conjugates was ~30 times lower than that of aPD-L1$_h$ (1.86×10^{-2} s^{-1} vs. 6.00×10^{-1} s^{-1}), supporting our first hypothesis that conjugation of aPD-L1$_h$ to dendrimers would significantly increase the PD-L1 binding. Note that the rupture forces higher than 50 pN were rarely detected from the control G7-Ac-COOH surface (**Figure 2E**), indicating that the interaction between the dendrimers and PD-L1 is negligible. In addition, BSA-immobilized probe exhibited significantly weaker interaction with the G7-aPD-L1$_h$ conjugates, compared to PD-L1-immobilized probe, further demonstrating a high specificity of the conjugates (**Figure S5**). Furthermore, the inverted configuration did not affect

the results, as the G7-aPD-L1$_h$-functionalized probe still showed stronger interactions with PD-L1 immobilized on the surface, compared to aPD-L1$_h$, although the results were statistically less significant (**Figure S6**). Note that discrepancy in k_{off} measured using BLI, SPR, and AFM have been commonly reported,[37] which is attributed to differences in experimental condition and detection sensitivity among such techniques. Particularly for AFM, the results could be affected by the parameters such as the number of molecules on the probe/surface.

The enhanced binding kinetics of the G7-aPD-L1$_h$ conjugates compared to aPD-L1$_h$ were then tested *in vitro* using the human renal cell carcinoma cancer cell line 786-O and breast cancer cell line MCF-7, which are known to express high and low levels of PD-L1, respectively.[38, 39] The western blot analysis of PD-L1 in these two cell lines confirmed significantly higher PD-L1 expression in 786-O, compared to MCF-7 (**Figure S7**). The target specificity of the G7-aPD-L1$_h$ conjugates was then examined by treating cells with 67 nM of inhibitor for 3 h, followed by staining with 4',6-Diamidino-2-Phenylindole (DAPI) on a nucleus. The expressions of aPD-L1$_h$ and the G7-aPD-L1$_h$ conjugates were both significantly higher on 786-O cells than MCF-7 cells (**Figure 3A**).

Next, we measured the *in vitro* binding affinity/avidity of the G7-aPD-L1$_h$ conjugates, which was compared to that of dendrimers without the antibodies (G7-Ac-COOH) and free aPD-L1$_h$, using a cell retention assay (**Figure 3B**).[40] A flow chamber (**Figure S8**), consisting of a basal PEGylated slide functionalized with either G7-Ac-COOH, aPD-L1$_h$, or the conjugates was used for the assay. Note that the amount of aPD-L1$_h$ immobilized on each surface was controlled to be comparable between the aPD-L1$_h$- and G7-aPD-L1$_h$-functionalized surfaces, by blocking the three fourths of surface reactive groups for immobilization of the G7-aPD-L1$_h$ conjugates (**Figure S9**). The detailed procedures are provided in **Supporting Information**. The BCA assay confirmed that

the amounts of antibodies immobilized on the both surfaces were equivalent (28 ± 7 ng/mm^2 vs. 27 ± 4 ng/mm^2 for G7-aPD-L1$_h$ vs. aPD-L1$_h$; p = .650) (**Figure S10**).

Cell retention was determined upon washing the cells at shear stresses of 0.36 or 3.6 dyne/cm^2 for 20 min, after 15 min incubation inside the chamber. The retention of PD-L1^{High} 786-O cells was significantly higher on the G7-aPD-L1$_h$-functinoalized surface, compared to the surface with free aPD-L1$_h$ (**Figure 3C** and **3D**). The difference was more significant at the higher flow rate, as only 0.4 ± 0.5% of 786-O cells were detached from the G7-aPD-L1$_h$-functionalized surface, which is a ~10-fold higher retention than the same surface without dendrimers (4.3 ± 1.2%; p<.001). These findings indicate the successful translation of the improved binding kinetics measured at the nanoscale into selective *in vitro* cell adhesion.

The higher retention observed on the G7-aPD-L1$_h$ surface, compared to aPD-L1$_h$, is likely due to an increase in local antibody density.[41, 42] Despite the equivalent number of antibodies presented on the both surfaces, the numerical analysis model (**Figure S11**) demonstrated a wider distribution in local antibody density on the G7-aPD-L1$_h$ surface than the aPD-L1$_h$ surface. This implies that the dendrimers cluster antibodies into a small, compacted area, forming an aPD-L1$_h$-concentrated region that effectively mediates strong multivalent binding. For PD-L1^{Low} MCF-7 cells, the cells displayed no noticeable difference in retention among the three surfaces, indicating that the G7-aPD-L1$_h$ conjugates have a high selectivity towards target proteins. Furthermore, over 96% of 786-O cells were washed away from the dendrimer-coated surface without antibodies, confirming that the G7-Ac-COOH do not induce cell binding.

In vitro/in vivo functional assays were conducted to confirm our second hypothesis: the increased binding kinetics would in turn improve the blockade of PD-1/PD-L1 interaction. We assessed the T cell interleukin-2 (IL-2) production and cancer cell chemoresistance to

doxorubicin (DOX), as described elsewhere.[4, 43, 44] The PD-1/PD-L1 interaction has been reported to affect T cell functions, including its cytokine production.[4] We quantitatively measured the amount of IL-2 secreted by PD-1 activated T cells via a coculture with cancer cells (**Figure 4A**). ELISA was utilized to assess IL-2 levels in the supernatants collected from two-day cocultures of cancer cells pre-treated with interferon-γ (IFN-γ, 10 ng/mL) and Jurkat T cells pre-treated with phorbol 12-myristate 13-acetate (PMA, 50 ng/mL)/phytohemagglutinin (PHA, 1 μg/mL). Different inhibitors, including the G7-aPD-L1$_h$ conjugates, aPD-L1$_h$, and G7-Ac-COOH, were applied to the IFN-γ-treated cancer cells at 33 nM, prior to the coculture. The IL-2 secretion from Jurkat T cells was observed to be the highest when 786-O cells were treated with the G7-aPD-L1$_h$ conjugates (**Figure 4B**). More specifically, G7-aPD-L1$_h$ increased the T cell IL-2 secretion by 1.9-fold ($p = 0.036$), which was ~35% more effective than aPD-L1$_h$ (1.4-fold increased; $p = 0.004$). Note that the dendrimer without antibodies did not affect the T cell IL-2 secretion ($p = 0.861$).

Recent reports suggest that chemotherapy in combination with PD-1/PD-L1 antagonists enhances antitumor effect, compared to chemotherapy alone.[43, 45] This is at least partially attributed to the fact that blockade of PD-1/PD-L1 interaction is known to prevent cancer cells from acquiring resistance to chemo-drugs.[43] The tumor cell lines were treated with the G7-aPD-L1$_h$ conjugates together with DOX, to investigate how enhanced binding kinetics of the conjugates to PD-L1 affects cytotoxicity of DOX (**Figure 4C**). Briefly, prior to co-culture with PD-1-activated T cells, the IFN-γ-treated cancer cells were incubated with G7-aPD-L1$_h$, aPD-L1$_h$, and G7-Ac-COOH, followed by Calcein-AM staining (see **Supporting Information** for details). Following 48 h of coculture, the cytotoxicity of DOX was measured by reduction of the Calcein-AM signal. As shown in **Figure 4D**, G7-aPD-L1$_h$ was more cytotoxic than aPD-L1$_h$ when used

in combination with DOX. For PD-L1^{High} 786-O cells, the cells pre-treated with G7-aPD-L1$_h$ and aPD-L1$_h$ demonstrated 1.6-fold ($p<0.001$) and 1.4-fold ($p<0.001$) greater cell death, respectively, than untreated cells. The dendrimers without antibodies did not display any noticeable cytotoxic effect ($p = 0.785$). Furthermore, the effect of PD-L1 blockade was not pronounced in MCF-7 cells, demonstrating *in vitro* selectivity of the dendrimer-ICI conjugates to PD-L1.

The *in vivo* behaviors of the G7-aPD-L1 conjugates were then tested using a tumor-bearing mouse model. For the *in vivo* study, mouse aPD-L1 (aPD-L1$_m$) was employed instead of aPD-L1$_h$, and the ratio of antibodies per dendrimer was increased to 9:1 in order to assure their selective tumor accumulation via stronger binding to PD-L1.[46] BCA assay demonstrated the molar ratio between dendrimers and antibodies to be 1:10. AFM images further revealed the larger size of the new conjugates, compared to the conjugates having ~3.7 antibodies per dendrimer (**Figure S12**). All the dendrimers and free antibodies were labeled with AF_{647}, to be fluorescently observed. Prior to the mouse model study, the *in vitro* selectivity of the G7-aPD-L1$_m$ conjugates to PD-L1$_m$ was confirmed using a mouse oral squamous cell carcinoma MOC1 cell line that overexpresses PD-L1.[47] As shown in **Figure 4E**, significant interactions of both aPD-L1$_m$ and G7-aPD-L1$_m$ with MOC1 cells were observed by the red fluorescence, while unconjugated dendrimers did not bind to the cells.

The G7-aPD-L1$_m$ conjugates were then applied to a MOC1 tumor-bearing mouse model. To establish the mouse tumor model, ~5×10^5 MOC1 cells were inoculated into nude mice (4- to 6-week-old; female). Once tumor size reached 300-500 mm^3, mice were randomized and 50 μL of either the G7-aPD-Ll$_m$ conjugates or aPD-L1$_m$ was injected through the tail vein at a concentration of ~128 nM (**Figure S12**). *In vivo* imaging system (IVIS) analysis after 72 hours injection revealed 2.5-fold ($p = 0.025$) increased targeting of the G7-aPD-L1$_m$ conjugates,

compared to aPD-L1$_m$ (**Figure 4F** and **4G**). Note that accumulation of the aPD-L1$_m$ was similar with that of G7-IgG$_m$, due to longer circulation half-life and less renal excretion of G7-IgG$_m$ which mediate strong passive targeting.[48, 49] The subsequent comparison of biodistribution analysis corroborated the target selectivity of the G7-aPD-L1$_m$ conjugates (**Figure 4H** and **4I**). The biodistribution of the three nanoparticles was not significantly different in other major organs, including brain, heart, lung, liver, kidney, and spleen. These findings suggested that the enhanced binding kinetics of the G7-aPD-L1$_m$ conjugates were successfully translated into *in vivo* selectivity. Obviously, our approach needs to be further validated by *in vivo* efficacy tests to confirm that the enhanced binding avidity through dendrimer-aPD-L1 conjugation is an effective method to improve the therapeutic efficacy of ICIs. An extensive *in vivo* study using syngeneic, immunocompetent mouse models will be the subject of our future publications.

In this study, we have engineered a nanotherapeutic platform which can effectively block PD-1/PD-L1 immune checkpoints by utilizing the multivalent binding effect mediated by hyperbranched dendrimers. The G7-aPD-L1 conjugates formed multiple binding pairs with PD-L1 proteins, creating significantly stronger interaction with the target receptors than free aPD-L1 did. This was confirmed using three direct measurement methods, BLI, SPR, and AFM, which all revealed that the G7-aPD-L1 conjugates achieved significantly enhanced binding avidity, compared to aPD-L1, by up to an order of magnitude. The enhancement in binding kinetics in turns increased the PD-L1 antagonist effect *in vitro*, as the dendrimer-ICI conjugates increased T-cell cytokine production while reducing cancer cell chemoresistance to DOX. The increased *in vivo* tumor accumulation of the G7-aPD-L1 conjugates further confirmed the enhanced target selectivity of the dendrimer-ICI conjugates towards the PD-L1 protein. Our current dendrimer-ICI system still has room for improvement to achieve even stronger targeting efficacy. For

example, the orientation of the surface-bound antibodies could be better controlled by utilizing a site-specific conjugation chemistry, such as sulfosuccinimidyl 4-(N-maleimidomethyl)cyclohexane-1-carboxylate (SMCC) and click chemistries. Nonetheless, despite the possibilities of having misoriented antibodies, we have demonstrated throughout the manuscript that the current system exhibits high enough binding avidity toward their target protein (**Figure S14**). In summary, the results presented in this study demonstrate that the dendrimer-mediated multivalent binding effect improves the blockade of immune checkpoints and has potential as a novel nanoscale platform for advanced cancer immunotherapy.

SCHEMES

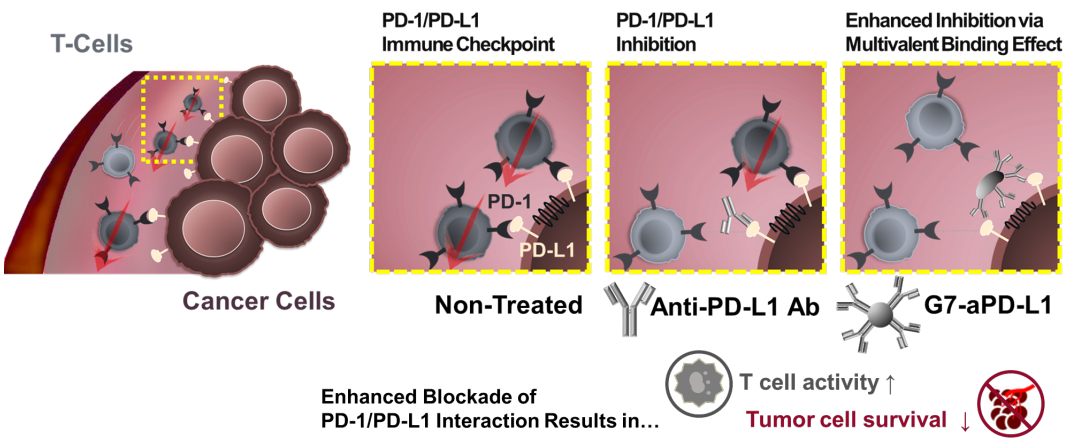

Scheme 1. A schematic diagram illustrating the hypothesis that the dendrimer-mediated multivalent interaction would substantially increase the antagonist effect of ICIs as a result of increased binding kinetics.

FIGURES

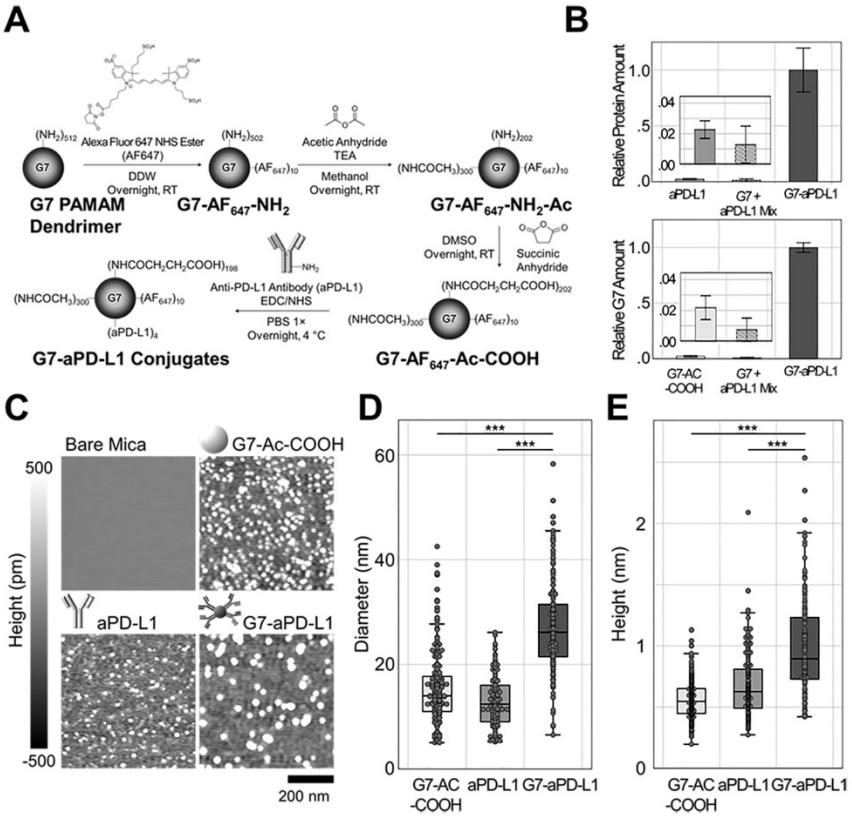

Figure 1. Synthesis and characterization of the G7-aPD-L1 conjugates. (A) Schematics describing the synthetic route of the G7-aPD-L1 conjugates. (B) The molar ratios of impurities, i.e., free antibodies (top) and non-conjugated dendrimers (bottom), after the conjugation reaction between G7-Ac-COOH and aPD-L1. Error bars represent standard deviations (SD). (C-E) The G7-aPD-L1 conjugates characterized using AFM. (C) AFM images of surface-adsorbed G7-Ac-COOH, aPD-L1$_h$, and G7-aPD-L1$_h$ conjugates, obtained in air. (D-E) Box plots for the diameters and heights of the nanoparticles obtained using AFM. The differences in height and diameter imply the flattening of the nanoparticles on the mica surface. Note that the center lines in box plots represent the median, boxes represent interquartile ranges (IQR), and error bars range from the first quartile (Q1) – 1.5 × IQR to Q3 + 1.5 × IQR.

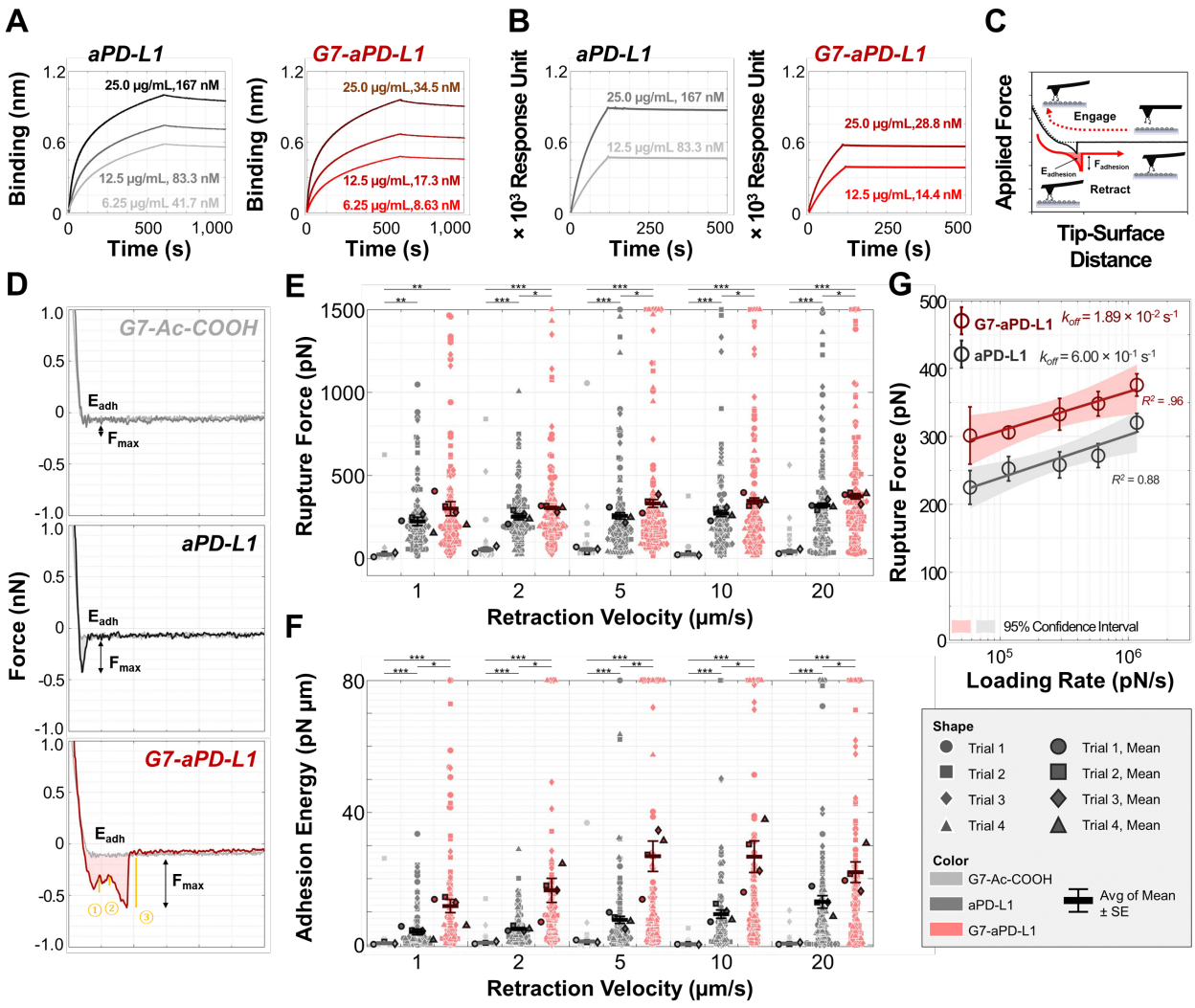

Figure 2. Binding kinetics of the dendrimer-aPD-L1 conjugates, free aPD-L1, and controls to PD-L1 quantitatively analyzed using three direct measurement methods: (A) BLI analysis; (B) SPR analysis; (C-G) AFM force spectroscopy. (C) A schematic diagram of the experimental set up for AFM analysis, representing the working principle of measuring dissociation kinetics between PD-L1 and its binding counterparts employed in this study. (D) Representative FD curves obtained from a PD-L1-immobilized probe, upon interaction with surfaces modified with G7-Ac-COOH (upper), aPD-L1h (middle), and G7-aPD-L1h (bottom). (E, F) Maximum

adhesion forces and adhesion energies collected from FD curves for interaction of probe-immobilized PD-L1 with surface-immobilized inhibitors. (G) Bell-Evans model fitting of the FD curves obtained at different pulling velocities. k_{off} values of the G7-aPD-L1$_h$ conjugates and free aPD-L1$_h$ were calculated as 1.86×10^{-2} s^{-1} and 6.00×10^{-1} s^{-1}, respectively. For (E-G), error bars represent standard error of mean.

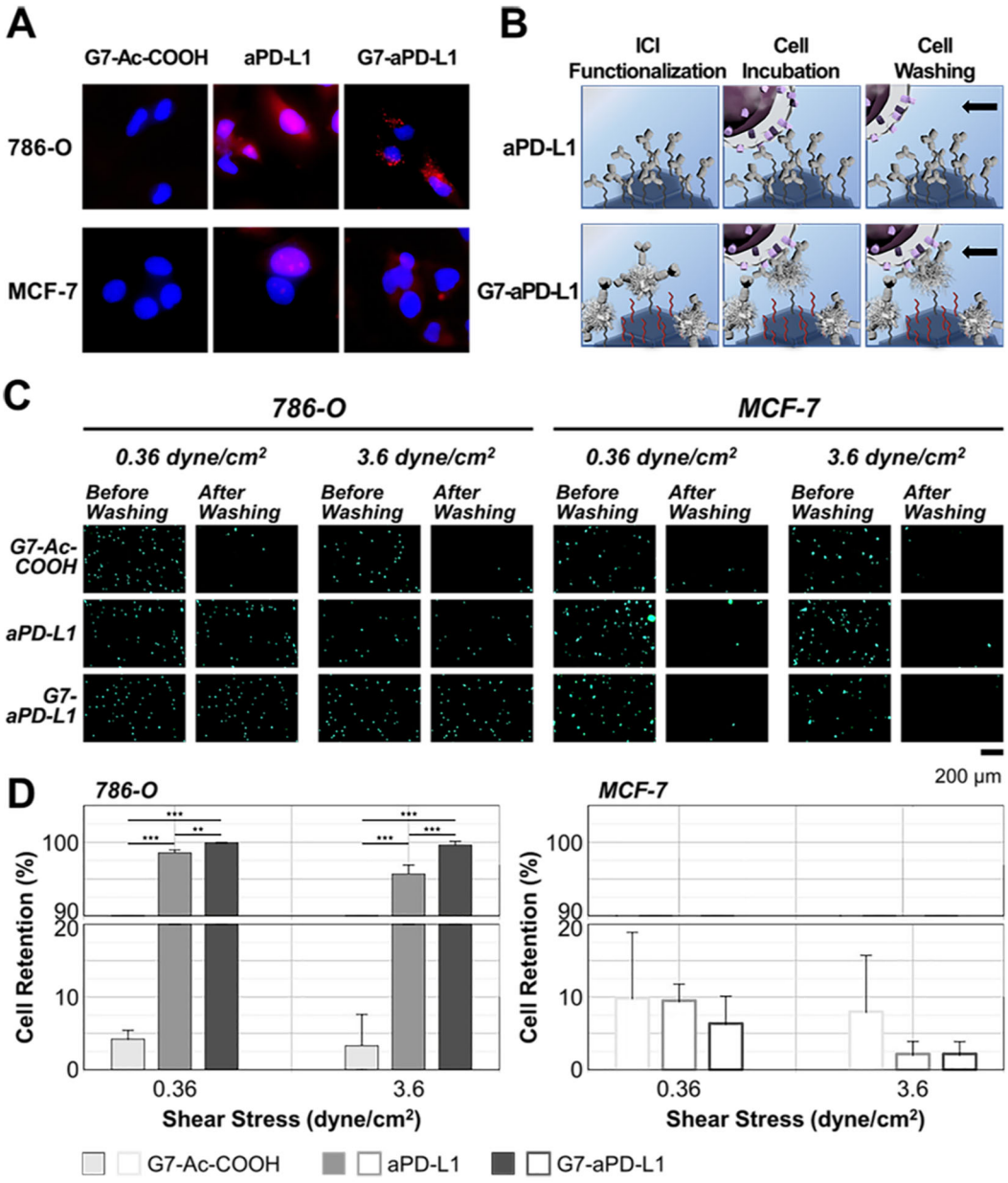

Figure 3. *In vitro* cell selectivity and enhanced binding avidity of the G7-aPD-L1$_h$ conjugates: (A) In vitro specificity of free aPD-L1 and the G7-aPD-L1$_h$ conjugates to PD-L1 observed using an inverted fluorescence microscope. (B-D) In vitro cell retention assay demonstrating the enhanced binding of the G7-aPD-L1$_h$ conjugates to PD-L1 expressing cells in a selective manner. An equivalent number of antibodies was immobilized on each of the aPD-L1$_h$ and G7-

aPD-L1$_h$ surfaces, whereas the dendrimer-coated surface without aPD-L1 (G7-Ac-COOH) was used as a negative control. The numbers of cells remained attached to the G7-Ac-COOH-, aPD-L1$_h$-, and G7-aPD-L1$_h$-functionalized surfaces were compared after exposure to shear stresses of 0.36 and 3.6 dyne/cm^2. All results indicate that the G7-aPD-L1$_h$ surfaces exhibit the strongest cell binding as a result of specific aPD-L1/PD-L1 adhesion. Error bars: SD.

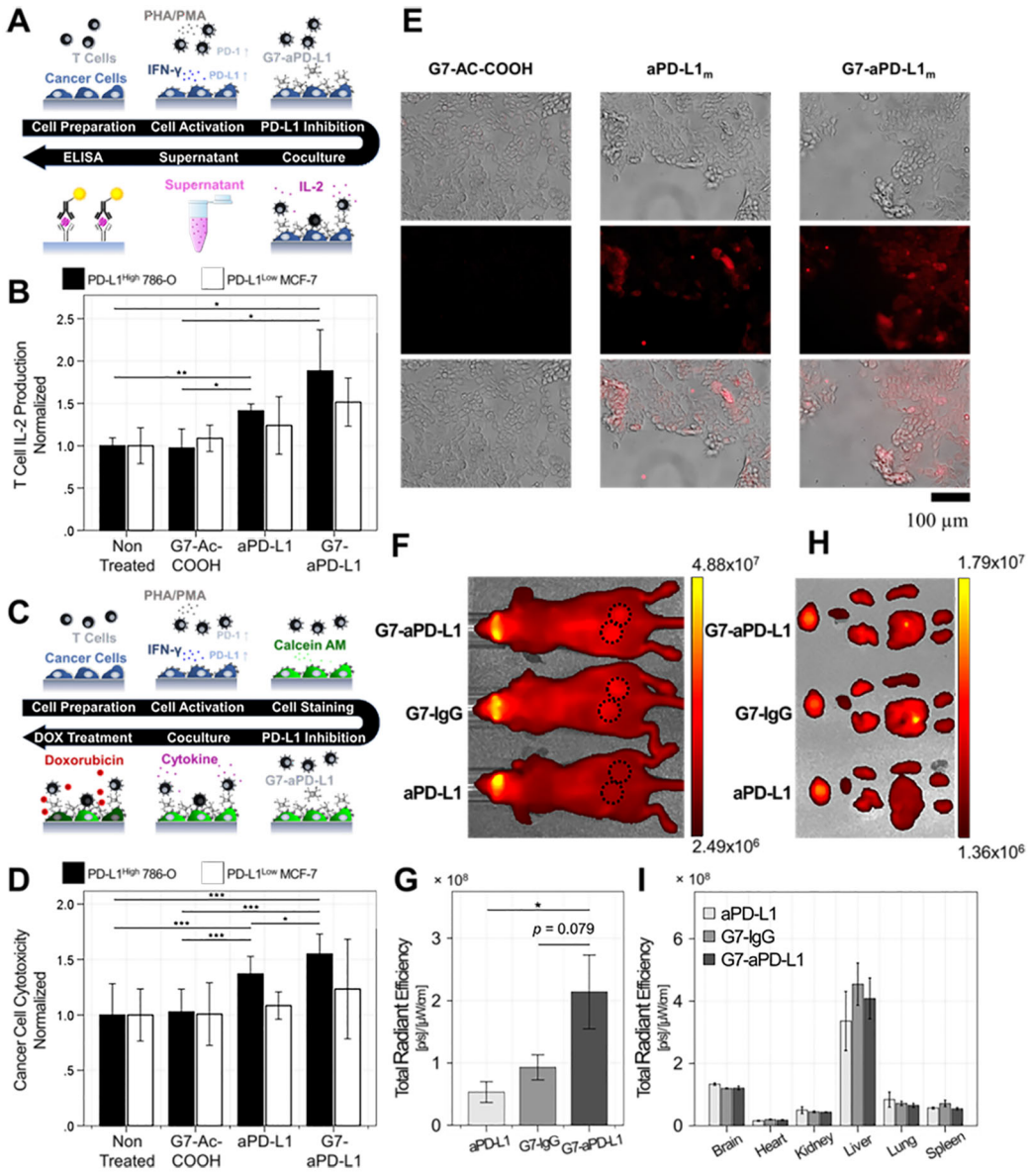

Figure 4. Enhanced *in vitro* PD-L1 blockade efficacy and *in vivo* selectivity of the G7-aPD-L1 conjugates compared to aPD-L1: (A, B) T cell IL-2 production assessed following the coculture of T cells and cancer cells (n = 3). Error bars represent standard deviation. (C, D) Cancer cell chemoresistance to DOX measured after coculturing the cells with the Jurkat T cells (n≥8). Note that cancer cells were pre-treated with either the G7-aPD-L1$_h$ conjugates, aPD-L1$_h$, or surface-modified dendrimers for A-D. Error bars: SD. (E) The *in vitro* target binding of the G7-aPD-

$L1_m$ conjugates confirmed using MOC1 cells. (F, G) *In vivo* imaging system (IVIS) analysis assessed using MOC1-tumor bearing mice (n = 8-10). Error bars represent standard error of means. (H, I) Biodistribution of the major organs and tumors obtained at 72 h after injection of the G7-aPD-conjugates. Error bars represent standard error of means.

ASSOCIATED CONTENT

Supporting Information Supporting information contains supplementary methods, results, and figures. This material is available free of charge via the Internet at http://pubs.acs.org

AUTHOR INFORMATION

Corresponding Author

Address all correspondence to:

Prof. Seungpyo Hong

Pharmaceutical Sciences Division, School of Pharmacy, University of Wisconsin-Madison

777 Highland Avenue, Madison, WI 53705, USA

email: seungpyo.hong@wisc.edu

phone: (608) 890-0699

Author Contributions

SH conceived the idea and provided experimental advice. SH and DLW provided funding support. SH and JB designed the project. JB, AN, MI designed, conceived, performed, and interpreted the experiments. WJ performed and interpreted the NMR spectra. AN performed and analyzed the GPC experiment and AFM imaging. WJ, KM, LJK, and EWL helped prepare the dendrimer-ICI conjugates. AN analyzed the AFM and GPC data. MJP collected data from BLI, SPR, and AFM force spectroscopies. JB designed, performed, and analyzed *in vitro* experiments. MI and DLW designed, performed, and analyzed *in vivo* tumor studies. JB, SH, and MI wrote the manuscript. All authors have given approval to the final version of the manuscript.

Funding Sources

This study was partially supported by NSF under grant # DMR-1808251 (SH). Research reported in this publication was also supported, in part, by pilot grants from the UW Carbone Cancer Center (DLW and SH, P30 CA014520) and Wisconsin Head & Neck Cancer SPORE (DLW and SH, P50 DE026787).

ACKNOWLEDGMENT

The authors would like to thank Yun Hwa Choi (UW-Madison) for her help in collecting the force measurement data.

ABBREVIATIONS

programmed death ligand 1, PD-L1; immune checkpoint inhibitor, anti-PD-L1 antibody, aPD-L1; G7 PAMAM dendrimer-aPD-L1 conjugates, G7-aPD-L1 conjugates; biolayer

interferometry, BLI; surface plasmon resonance spectroscopy, SPR; atomic force microscopy, AFM; proton nuclear magnetic resonance, ^{1}H NMR; N-hydroxysuccinimide, NHS; bicinchoninic acid assay, BCA assay; gel permeation chromatography, GPC; interleukin-2, IL-2; interferon-γ, IFN-γ; doxorubicin, DOX.

REFERENCES

1. Whiteside, T. L. Immune Suppression in Cancer: Effects on Immune Cells, Mechanisms and Future Therapeutic Intervention. *Semin. Cancer. Biol.* **2006,** *16* (1), 3-15.
2. Konstantinidou, M.; Zarganes-Tzitzikas, T.; Magiera-Mularz, K.; Holak, T. A.; Dömling, A. Immune Checkpoint PD-1/PD-L1: Is There Life Beyond Antibodies? *Angew. Chem. Int. Ed. Engl.* **2018,** *57* (18), 4840-4848.
3. Keir, M. E.; Butte, M. J.; Freeman, G. J.; Sharpe, A. H. PD-1 and Its Ligands in Tolerance and Immunity. *Annu. Rev. Immunol.* **2008,** *26*, 677-704.
4. Yang, W.; Chen, P. W.; Li, H.; Alizadeh, H.; Niederkorn, J. Y. PD-L1: PD-1 Interaction Contributes to the Functional Suppression of T-Cell Responses to Human Uveal Melanoma Cells in Vitro. *Investig. Ophthalmol. Vis. Sci.* **2008,** *49* (6), 2518-2525.
5. Sun, J.; Xu, K.; Wu, C.; Wang, Y.; Hu, Y.; Zhu, Y.; Chen, Y.; Shi, Q.; Yu, G.; Zhang, X. PD-L1 Expression Analysis in Gastric Carcinoma Tissue and Blocking of Tumor-Associated PD-L1 Signaling by Two Functional Monoclonal Antibodies. *Tissue Antigens* **2007,** *69* (1), 19-27.
6. Thalya, B.; Jon, E.; Fister, K. R. Optimal Control Applied to Immunotherapy. *Discrete Contin. Dyn.-B* **2003,** *4* (1), 135-146.
7. Rodell, C. B.; Arlauckas, S. P.; Cuccarese, M. F.; Garris, C. S.; Li, R.; Ahmed, M. S.; Kohler, R. H.; Pittet, M. J.; Weissleder, R. TLR7/8-Agonist-Loaded Nanoparticles Promote the Polarization of Tumour-Associated Macrophages to Enhance Cancer Immunotherapy. *Nat. Biomed. Eng.* **2018,** *2* (8), 578-588.
8. Choo, Y. W.; Kang, M.; Kim, H. Y.; Han, J.; Kang, S.; Lee, J.-R.; Jeong, G.-J.; Kwon, S. P.; Song, S. Y.; Go, S.; Jung, M.; Hong, J.; Kim, B.-S. M1 Macrophage-Derived Nanovesicles Potentiate the Anticancer Efficacy of Immune Checkpoint Inhibitors. *ACS Nano* **2018,** *12* (9), 8977-8993.
9. Dai, L.; Li, K.; Li, M.; Zhao, X.; Luo, Z.; Lu, L.; Luo, Y.; Cai, K. Size/Charge Changeable Acidity-Responsive Micelleplex for Photodynamic-Improved PD-L1 Immunotherapy with Enhanced Tumor Penetration. *Adv. Funct. Mater.* **2018,** *28* (18), 1707249.
10. Guan, X.; Chen, J.; Hu, Y.; Lin, L.; Sun, P.; Tian, H.; Chen, X. Highly Enhanced Cancer Immunotherapy by Combining Nanovaccine with Hyaluronidase. *Biomaterials* **2018,** *171*, 198-206.
11. Lozano, T.; Soldevilla, M. M.; Casares, N.; Villanueva, H.; Bendandi, M.; Lasarte, J. J.; Pastor, F. Targeting Inhibition of Foxp3 by a CD28 2′-Fluro Oligonucleotide Aptamer

Conjugated to P60-Peptide Enhances Active Cancer Immunotherapy. *Biomaterials* **2016,** *91*, 73-80.
12. D'Incecco, A.; Andreozzi, M.; Ludovini, V.; Rossi, E.; Capodanno, A.; Landi, L.; Tibaldi, C.; Minuti, G.; Salvini, J.; Coppi, E.; Chella, A.; Fontanini, G.; Filice, M. E.; Tornillo, L.; Incensati, R. M.; Sani, S.; Crinò, L.; Terracciano, L.; Cappuzzo, F. PD-1 and PD-L1 Expression in Molecularly Selected Non-Small-Cell Lung Cancer Patients. *Br. J. Cancer* **2015,** *112* (1), 95-102.
13. Hamanishi, J.; Mandai, M.; Iwasaki, M.; Okazaki, T.; Tanaka, Y.; Yamaguchi, K.; Higuchi, T.; Yagi, H.; Takakura, K.; Minato, N.; Honjo, T.; Fujii, S. Programmed Cell Death 1 Ligand 1 and Tumor-Infiltrating CD8+ T Lymphocytes Are Prognostic Factors of Human Ovarian Cancer. *Proc. Natl. Acad. Sci. U. S. A.* **2007,** *104* (9), 3360-5.
14. Liu, C. Q.; Xu, J.; Zhou, Z. G.; Jin, L. L.; Yu, X. J.; Xiao, G.; Lin, J.; Zhuang, S. M.; Zhang, Y. J.; Zheng, L. Expression Patterns of Programmed Death Ligand 1 Correlate with Different Microenvironments and Patient Prognosis in Hepatocellular Carcinoma. *Br. J. Cancer* **2018,** *119* (1), 80-88.
15. Nakanishi, J.; Wada, Y.; Matsumoto, K.; Azuma, M.; Kikuchi, K.; Ueda, S. Overexpression of B7-H1 (PD-L1) Significantly Associates with Tumor Grade and Postoperative Prognosis in Human Urothelial Cancers. *Cancer Immunol. Immunother.* **2007,** *56* (8), 1173-82.
16. Gao, Q.; Wang, X. Y.; Qiu, S. J.; Yamato, I.; Sho, M.; Nakajima, Y.; Zhou, J.; Li, B. Z.; Shi, Y. H.; Xiao, Y. S.; Xu, Y.; Fan, J. Overexpression of PD-L1 Significantly Associates with Tumor Aggressiveness and Postoperative Recurrence in Human Hepatocellular Carcinoma. *Clin. Cancer Res.* **2009,** *15* (3), 971-9.
17. Hargadon, K. M.; Johnson, C. E.; Williams, C. J. Immune Checkpoint Blockade Therapy for Cancer: An Overview of FDA-Approved Immune Checkpoint Inhibitors. *Int. Immunopharmacol.* **2018,** *62*, 29-39.
18. Brahmer, J. R.; Tykodi, S. S.; Chow, L. Q. M.; Hwu, W.-J.; Topalian, S. L.; Hwu, P.; Drake, C. G.; Camacho, L. H.; Kauh, J.; Odunsi, K.; Pitot, H. C.; Hamid, O.; Bhatia, S.; Martins, R.; Eaton, K.; Chen, S.; Salay, T. M.; Alaparthy, S.; Grosso, J. F.; Korman, A. J.; Parker, S. M.; Agrawal, S.; Goldberg, S. M.; Pardoll, D. M.; Gupta, A.; Wigginton, J. M. Safety and Activity of Anti-PD-L1 Antibody in Patients with Advanced Cancer. *N. Engl. J. Med.* **2012,** *366* (26), 2455-2465.
19. Ventola, C. L. Cancer Immunotherapy, Part 3: Challenges and Future Trends. *P & T : a peer-reviewed journal for formulary management* **2017,** *42* (8), 514-521.
20. Kosmides, A. K.; Sidhom, J.-W.; Fraser, A.; Bessell, C. A.; Schneck, J. P. Dual Targeting Nanoparticle Stimulates the Immune System To Inhibit Tumor Growth. *ACS Nano* **2017,** *11* (6), 5417-5429.
21. Munari, E.; Zamboni, G.; Lunardi, G.; Marchionni, L.; Marconi, M.; Sommaggio, M.; Brunelli, M.; Martignoni, G.; Netto, G. J.; Hoque, M. O.; Moretta, F.; Mingari, M. C.; Pegoraro, M. C.; Inno, A.; Paiano, S.; Terzi, A.; Cavazza, A.; Rossi, G.; Mariotti, F. R.; Vacca, P.; Moretta, L.; Bogina, G. PD-L1 Expression Heterogeneity in Non–Small Cell Lung Cancer: Defining Criteria for Harmonization between Biopsy Specimens and Whole Sections. *J. Thorac. Oncol.* **2018,** *13* (8), 1113-1120.
22. Wang, H.; Yao, H.; Li, C.; Shi, H.; Lan, J.; Li, Z.; Zhang, Y.; Liang, L.; Fang, J.-Y.; Xu, J. HIP1R Targets PD-L1 to Lysosomal Degradation to Alter T cell–Mediated Cytotoxicity. *Nat. Chem. Biol.* **2019,** *15* (1), 42-50.

23. Chowdhury, S.; Veyhl, J.; Jessa, F.; Polyakova, O.; Alenzi, A.; MacMillan, C.; Ralhan, R.; Walfish, P. G. Programmed Death-Ligand 1 Overexpression Is a Prognostic Marker for Aggressive Papillary Thyroid Cancer and Its Variants. *Oncotarget* **2016***; 7(22),* 32318-32328.
24. Myung, J. H.; Gajjar, K. A.; Saric, J.; Eddington, D. T.; Hong, S. Dendrimer-Mediated Multivalent Binding for the Enhanced Capture of Tumor Cells. *Angew. Chem. Int. Ed. Engl.* **2011,** *50* (49), 11769-11772.
25. Poellmann, M. J.; Bu, J.; Hong, S. Would Antioxidant-Loaded Nanoparticles Present an Effective Treatment for Ischemic Stroke? *Nanomedicine (Lond.)* **2018,** *13* (18), 2327-2340.
26. Jeong, W.-J.; Bu, J.; Kubiatowicz, L. J.; Chen, S. S.; Kim, Y.; Hong, S. Peptide-Nanoparticle Conjugates: A Next Generation of Diagnostic and Therapeutic Platforms? *Nano Converg.* **2018,** *5* (1), 38-38.
27. Xie, J.; Wang, J.; Chen, H.; Shen, W.; Sinko, P. J.; Dong, H.; Zhao, R.; Lu, Y.; Zhu, Y.; Jia, L. Multivalent Conjugation of Antibody to Dendrimers for the Enhanced Capture and Regulation on Colon Cancer Cells. *Scientific Reports* **2015,** *5*, 9445.
28. Jeong, W.-j.; Bu, J.; Han, Y.; Drelich, A. J.; Nair, A.; Král, P.; Hong, S. Nanoparticle Conjugation Stabilizes and Multimerizes β-Hairpin Peptides To Effectively Target PD-1/PD-L1 β-Sheet-Rich Interfaces. *J. Am. Chem. Soc.* **2020,** *142* (4), 1832-1837.
29. Khandare, J.; Kolhe, P.; Pillai, O.; Kannan, S.; Lieh-Lai, M.; Kannan, R. M. Synthesis, Cellular Transport, and Activity of Polyamidoamine Dendrimer-Methylprednisolone Conjugates. *Bioconjug. Chem.* **2005,** *16* (2), 330-337.
30. Li, J.; Piehler, L. T.; Qin, D.; Baker, J. R.; Tomalia, D. A.; Meier, D. J. Visualization and Characterization of Poly(amidoamine) Dendrimers by Atomic Force Microscopy. *Langmuir* **2000,** *16* (13), 5613-5616.
31. Gestwicki, J. E.; Cairo, C. W.; Mann, D. A.; Owen, R. M.; Kiessling, L. L. Selective Immobilization of Multivalent Ligands for Surface Plasmon Resonance and Fluorescence Microscopy. *Anal. Biochem.* **2002,** *305* (2), 149-55.
32. Poellmann, M. J.; Nair, A.; Bu, J.; Kim, J. K. H.; Kimple, R. J.; Hong, S., Immunoavidity-Based Capture of Tumor Exosomes Using Poly(amidoamine) Dendrimer Surfaces. *Nano Letters* **2020**.
33. Ratto, T. V.; Rudd, R. E.; Langry, K. C.; Balhorn, R. L.; McElfresh, M. W., Nonlinearly additive forces in multivalent ligand binding to a single protein revealed with force spectroscopy. *Langmuir* **2006,** *22* (4), 1749-57.
34. Sulchek, T.; Friddle, R. W.; Noy, A. Strength of Multiple Parallel Biological Bonds. *Biophys. J.* **2006,** *90* (12), 4686-91.
35. Leistra, A. N.; Han, J. H.; Tang, S.; Orr, B. G.; Banaszak Holl, M. M.; Choi, S. K.; Sinniah, K. Force Spectroscopy of Multivalent Binding of Riboflavin-Conjugated Dendrimers to Riboflavin Binding Protein. *J. Phys. Chem. B* **2015,** *119* (18), 5785-92.
36. Evans, E.; Ritchie, K. Dynamic Strength of Molecular Adhesion Bonds. *Biophys. J.* **1997,** *72* (4), 1541-55.
37. Casillas-Ituarte, N. N.; Cruz, C. H. B.; Lins, R. D.; DiBartola, A. C.; Howard, J.; Liang, X.; Höök, M.; Viana, I. F. T.; Sierra-Hernández, M. R.; Lower, S. K., Amino acid polymorphisms in the fibronectin-binding repeats of fibronectin-binding protein A affect bond strength and fibronectin conformation. *J. Biol.* **2017,** *292* (21), 8797-8810.

38. Mittendorf, E. A.; Philips, A. V.; Meric-Bernstam, F.; Qiao, N.; Wu, Y.; Harrington, S.; Su, X.; Wang, Y.; Gonzalez-Angulo, A. M.; Akcakanat, A.; Chawla, A.; Curran, M.; Hwu, P.; Sharma, P.; Litton, J. K.; Molldrem, J. J.; Alatrash, G. PD-L1 Expression in Triple-Negative Breast Cancer. *Cancer Immunol. Res.* **2014,** *2* (4), 361-70.
39. Zhu, Q.; Cai, M. Y.; Weng, D. S.; Zhao, J. J.; Pan, Q. Z.; Wang, Q. J.; Tang, Y.; He, J.; Li, M.; Xia, J. C. PD-L1 Expression Patterns in Tumour Cells and Their Association with CD8. *J. Cancer* **2019,** *10* (5), 1154-1161.
40. Myung, J. H.; Eblan, M. J.; Caster, J. M.; Park, S. J.; Poellmann, M. J.; Wang, K.; Tam, K. A.; Miller, S. M.; Shen, C.; Chen, R. C.; Zhang, T.; Tepper, J. E.; Chera, B. S.; Wang, A. Z.; Hong, S., Multivalent Binding and Biomimetic Cell Rolling Improves the Sensitivity and Specificity of Circulating Tumor Cell Capture. *Clin. Cancer Res.* **2018,** *24* (11), 2539-2547.
41. Myung, J. H.; Roengvoraphoj, M.; Tam, K. A.; Ma, T.; Memoli, V. A.; Dmitrovsky, E.; Freemantle, S. J.; Hong, S. Effective Capture of Circulating Tumor Cells from a Transgenic Mouse Lung Cancer Model Using Dendrimer Surfaces Immobilized with Anti-EGFR. *Anal. Chem.* **2015,** *87* (19), 10096-102.
42. Bu, J.; Nair, A.; Kubiatowicz, L. J.; Poellmann, M. J.; Jeong, W.-j.; Reyes-Martinez, M.; Armstrong, A. J.; George, D. J.; Wang, A. Z.; Zhang, T.; Hong, S., Surface engineering for efficient capture of circulating tumor cells in renal cell carcinoma: From nanoscale analysis to clinical application. *Biosens. Bioelectron.* **2020**, 112250.
43. Black, M.; Barsoum, I. B.; Truesdell, P.; Cotechini, T.; Macdonald-Goodfellow, S. K.; Petroff, M.; Siemens, D. R.; Koti, M.; Craig, A. W.; Graham, C. H., Activation of the PD-1/PD-L1 immune checkpoint confers tumor cell chemoresistance associated with increased metastasis. *Oncotarget* **2016,** *7* (9), 10557-67.
44. Burr, M. L.; Sparbier, C. E.; Chan, Y. C.; Williamson, J. C.; Woods, K.; Beavis, P. A.; Lam, E. Y. N.; Henderson, M. A.; Bell, C. C.; Stolzenburg, S.; Gilan, O.; Bloor, S.; Noori, T.; Morgens, D. W.; Bassik, M. C.; Neeson, P. J.; Behren, A.; Darcy, P. K.; Dawson, S. J.; Voskoboinik, I.; Trapani, J. A.; Cebon, J.; Lehner, P. J.; Dawson, M. A., CMTM6 Maintains the Expression of PD-L1 and Regulates Anti-Tumour Immunity. *Nature* **2017,** *549* (7670), 101-105.
45. Sun, D.; Ma, J.; Wang, J.; Han, C.; Qian, Y.; Chen, G.; Li, X.; Zhang, J.; Cui, P.; Du, W.; Wu, Z.; Chen, S.; Zheng, X.; Yue, Z.; Song, J.; Gao, C.; Zhao, X.; Cai, S.; Hu, Y., Anti-PD-1 therapy combined with chemotherapy in patients with advanced biliary tract cancer. *Cancer. Immunol. Immunother.* **2019,** *68* (9), 1527-1535.
46. Sykes, E. A.; Chen, J.; Zheng, G.; Chan, W. C. W., Investigating the Impact of Nanoparticle Size on Active and Passive Tumor Targeting Efficiency. *ACS Nano* **2014,** *8* (6), 5696-5706.
47. Moore, E. C.; Cash, H. A.; Caruso, A. M.; Uppaluri, R.; Hodge, J. W.; Van Waes, C.; Allen, C. T., Enhanced Tumor Control with Combination mTOR and PD-L1 Inhibition in Syngeneic Oral Cavity Cancers. *Cancer Immunol. Res.* **2016,** *4* (7), 611-620.
48. Sunoqrot, S.; Bugno, J.; Lantvit, D.; Burdette, J. E.; Hong, S. Prolonged Blood Circulation and Enhanced Tumor Accumulation of Folate-Targeted Dendrimer-Polymer Hybrid Nanoparticles. *J. Control Release* **2014,** *191*, 115-122.
49. Attia, M. F.; Anton, N.; Wallyn, J.; Omran, Z.; Vandamme, T. F., An overview of active and passive targeting strategies to improve the nanocarriers efficiency to tumour sites. *J. Pharm. Pharmacol.* **2019,** *71* (8), 1185-1198.